The Astrophysical Journal, 634:679–686, 2005 November 20

FIRST TESTS OF WAVEFRONT SENSING WITH A CONSTELLATION OF LASER GUIDE BEACONS

M. Lloyd-Hart, C. Baranec, N. M. Milton, T. Stalcup, M. Snyder, N. Putnam, and J. R. P. Angel
Steward Observatory, University of Arizona, 933 North Cherry Avenue, Tucson, AZ 85721; mhart@as.arizona.edu
Received 2005 July 15; accepted 2005 August 3

ABSTRACT

Adaptive optics to correct current telescopes over wide fields, or even to correct future very large telescopes over narrow fields, will require real-time wavefront measurements made with a constellation of laser beacons. Here we report the first such measurements, made at the 6.5 m MMT with five Rayleigh beacons in a 2′ pentagon. Each beacon is made with a pulsed beam at 532 nm of 4 W at the exit pupil of the projector. The return is range-gated from 20 to 29 km and recorded at 53 Hz by a 36-element Shack-Hartmann sensor. Wavefronts derived from the beacons are compared with simultaneous wavefronts obtained for individual natural stars within or near the constellation. Observations were made in seeing averaging 1.″0 with two-thirds of the aberration measured to be from a ground layer of mean height 380 m. Under these conditions, subtraction of the simple instantaneous average of the five beacon wavefronts from the stellar wavefronts yielded a 40% rms reduction in the measured modes of the distortion over a 2′ field. We discuss the use of multiple Rayleigh beacons as an alternative to single sodium beacons on 8 m telescopes and the impact of the new work on the design of a multi–sodium beacon system for the 25 m Giant Magellan Telescope.

Subject headings: atmospheric effects — instrumentation: adaptive optics — instrumentation: high angular resolution — telescopes

Online material: mpeg animation

1. INTRODUCTION

Ground-based astronomical telescopes with adaptive correction are able to exceed the resolution of the *Hubble Space Telescope*. However, their use is currently limited almost exclusively to a small fraction of the sky, in small fields of view around the stars required to measure the wavefront error. These stars must be relatively bright because removal of atmospheric blurring requires rapidly updated command signals to the wavefront corrector. The radius of the compensated field around the star, the isoplanatic angle, is limited because atmospheric turbulence extends many kilometers above the ground, so the integrated wavefront distortion depends sensitively on the direction of view.

For telescopes in the current 8–10 m class, the limitation on brightness, although not on corrected field of view, can be largely removed by use of a laser beam projected toward a faint astronomical target to create an artificial beacon. Light from a sodium resonance beacon generated at ~90 km altitude follows the path taken by light from the target closely enough that a good estimate of the aberrations in the latter can be derived. The laser light, however, does not come from infinity, and as the telescope diameter is increased, the mismatch in optical paths (the cone effect) eventually becomes so severe that no useful recovery of stellar wavefronts can be made.

Extremely large telescopes (ELTs) with diameters greater than 25 m will therefore require a further advance to recover diffraction-limited imaging with adaptive optics (AO). Multiple beacons placed so that their light collectively samples the full volume of atmosphere traversed by light from a target could in principle provide the solution. The instantaneous stellar wavefront would be computed by a tomographic algorithm applied to the wavefronts measured from all the beacons (Ragazzoni et al. 1999; Tokovinin et al. 2001; Lloyd-Hart & Milton 2003b). This method, implemented with sodium beacon lasers, is planned for the Giant Magellan Telescope (GMT; Milton et al. 2003) and for the Thirty Meter Telescope (Dekany et al. 2004) to recover the full resolution of their apertures.

In the simplest application of tomography, the stellar wavefront along a single line of sight is estimated from all the measured beacon wavefronts, and the compensating phase is applied to a single deformable mirror (DM). The technique, called laser tomography AO (LTAO), delivers a diffraction-limited field of view limited by the normal isoplanatic angle.

Once a telescope is equipped with multiple laser beacons and tomographic analysis, a variety of altitude-conjugated AO techniques are enabled: diffraction-limited resolution over a field many times the isoplanatic angle with multiconjugate and multiobject AO (MCAO and MOAO; Beckers 1988; Tokovinin et al. 2000; Hammer et al. 2002; Dekany et al. 2004) and partially improved seeing over a yet larger field with ground-layer AO (GLAO).

Of these advanced techniques, only MCAO has yet been attempted, in experiments at two solar telescopes (Langlois et al. 2004; Berkefeld et al. 2004). Numerical models of GLAO based on measurements of the vertical distribution of turbulence at a number of sites (Rigaut 2002; Tokovinin 2004a, 2004b) suggest the potential for dramatic image improvement in the near-infrared. D. R. Anderson et al. (2005, in preparation) have modeled GLAO performance in detail, using vertical distributions of turbulence seen at Cerro Pachòn that put roughly two-thirds of the power in the ground layer. With a pentagonal arrangement of laser guide stars (LGSs) and an adaptive secondary mirror, the study concluded that the median image width in the *K* band would improve from 0.″42 to 0.″18 for a 5′ field and to 0.″25 for a field of 10′.

Ground-breaking work by Ragazzoni et al. (2000) has hinted at the power of tomographic wavefront sensing. That paper describes the first experiments in tomography, at the Telescopio Nazionale Galileo, in which wavefront estimates were obtained simultaneously from a close asterism of four natural stars through the simple expedient of defocusing the telescope. The instantaneous Zernike modal amplitudes measured from one star were compared to estimates derived from the modal amplitudes of the other three. Tomographic estimation from the three beacon stars was shown to be substantially superior to a simple average or the use of any one of the three individually.

We report in this paper results from the first implementation of a wavefront sensing system based on a constellation of multiple laser beacons. Previous work on laser-guided AO has been confined to a single beacon, usually created by resonance scattering in the sodium layer at 90 km altitude (Gavel et al. 2000; Fugate 2003; Wizinowich et al. 2004). For our work at the 6.5 m MMT (Multiple Mirror Telescope) we have created five beacons generated by Rayleigh scattering. Commercial, pulsed doubled-YAG (yttrium aluminum garnet) lasers at 532 nm are used, readily available at moderate cost. Single Rayleigh beacons gated to an altitude of ~12 km have previously been used for AO with small telescopes (Fugate et al. 1991), but the strong focus anisoplanatism and incomplete sampling of higher turbulence make a single such beacon of little value for an 8 m class telescope.

For our experiments, however, Rayleigh beacons are ideal. In our system the range gate is centered at 24 km altitude, high enough to collectively sample most of the turbulence. To increase signal strength, the sensor system includes optics to focus the telescope dynamically, to maintain sharp images of each laser pulse at it rises from 20 to 29 km (Georges et al. 2003; Stalcup et al. 2004). In this way, the range gate is extended to ~20 times longer than the telescope's normal depth of field. Even at this high altitude, focus anisoplanatism would remain a difficulty with a single beacon, but with five it is not an issue, precisely because our goal is the development of tomographic techniques. The practical advantage is that the current high capital and operating costs of tuned sodium lasers for resonance scattering are avoided, allowing us to make an early start.

2. INSTRUMENT DESCRIPTION

The multibeacon experiment at the MMT has been designed to investigate both full tomographic wavefront sensing needed for diffraction-limited imaging and ground-layer sensing to improve the seeing. With these goals in mind and guided by previous modeling of tomography (Lloyd-Hart & Milton 2003a), we have built a pentagonal constellation of Rayleigh laser guide stars (RLGSs) with a diameter of 2′. This field is not as large as one would choose for ground-layer sensing alone, given theoretical predictions of the size of the field that could be corrected by a GLAO system; nevertheless, it is capable of taking the first steps to quantifying the degree of correction to be expected of a closed-loop system.

The experimental setup divides into two parts: the lasers and beam projector optics to generate the five RLGSs and the wavefront sensor (WFS) detectors and associated optics mounted at the telescope's Cassegrain focus.

2.1. *Generating the Laser Guide Stars*

The mean range chosen for the Rayleigh return is 24 km, where the beacons form a pentagon 14 m in diameter. The collective volume filling of this arrangement allows for three-dimensional sensing of the turbulence by tomography for ranges up to 10 km and thus avoids the focal anisoplanatism that would arise from a single RLGS.

The projection system employs two frequency-doubled YAG lasers from Lightwave Electronics, rated at a nominal 15 W output each, operating at 532 nm and 5 kHz pulse repetition rate (Stalcup et al. 2004). The two linearly polarized beams are combined with a polarizing beam splitter to produce a single, diffraction-limited beam measured at ~27 W. In operation, synchronized pulses of light from the lasers are split by a computer-generated hologram in the projection optics to create the five beacons on a 2′ diameter ring on the sky. The lasers and combining optics are attached directly to the 6.5 m telescope tube, with the power supplies and chiller in an adjacent room in the corotating MMT building. The laser heads are in a thermally controlled enclosure. At the top of the telescope tube on one side is a steering mirror close to an image of the exit pupil, used to compensate for slow misalignments in the projected beam direction caused by flexure and temperature changes. The hologram is also at this pupil. The beams are launched together through a single 50 cm diameter telephoto objective lens mounted centrally on the 6.5 m telescope axis, directly above the secondary mirror.

2.2. *Cassegrain Instrument for Wavefront Sensing*

The WFS package mounts at the MMT's Cassegrain focus and includes distinct optical arms for the RLGSs and a natural star. The first comprises a novel sensor, which includes the dynamic focus optics, described in detail in Georges et al. (2003), and a single electronically shuttered CCD, which images all five beacons.

We aim to measure laser returns from ~24 km altitude, twice the height of earlier Rayleigh beacons (Fugate et al. 1991), to allow better sampling of high turbulent layers. Because the air at that altitude is only 10% of the sea-level density, we have developed a new technology to focus the telescope continuously to follow the rising pulse from a Q-switched laser (Angel & Lloyd-Hart 2000; Lloyd-Hart et al. 2002). The sensitivity is thereby increased by an order of magnitude compared to conventional range-gating methods. The dynamic focus of all five beacons is achieved by sinusoidal motion of a single 25 mm mirror placed at an image of the telescope pupil, with approximately one-third of each cycle matched to the motion of the returning laser pulse.

The dynamic focus optics and mechanical resonator that moves the mirror are included in the foreoptics of the RLGS sensor. The resonator also serves as the system's master clock, triggering the laser pulses and the RLGS WFS detector shutter at prescribed phase delays. In this way, each laser pulse is tracked in focus over a range gate from 20 to 29 km.

The refocused laser light is imaged onto a common 35 mm pupil, where a prism array (Putnam et al. 2004) divides the light into 36 subapertures of equal size in a hexapolar geometry. A compound lens following the prism array images the beacons into five separate 36-spot Shack-Hartmann patterns on the detector, a CCID18 from Lincoln Laboratory. This is a 128×128 pixel frame transfer device with 16 output amplifiers and an electronic shutter. The controller, supplied by SciMeasure, reads the detector at frame rates up to 915 Hz. Operation of the electronic shutter during transitions of the CCD clock signals introduces additional noise into the image, so a carefully interleaved sequence is required of the clocks, for the frame transfer and read operations, and of the shutter, which is triggered by the dynamic focus oscillator.

In order to explore the effectiveness of the RLGS WFS as a function of position within the field, a second optical arm of the Cassegrain instrument was built with a standard Shack-Hartmann sensor to measure wavefronts from natural stars. A dichroic splitter covering a 3′ field separates the beams to the two WFSs, transmitting the laser light to the LGS arm and reflecting starlight at wavelengths longward of 650 nm to the star sensor.

The star WFS is a copy of the one normally used for adaptive optics with the MMT adaptive secondary mirror (Brusa et al. 2004). The pupil is divided into a 12×12 array of square subapertures of which 108 are illuminated. The camera uses an E2V CCD39 frame transfer detector with 80×80 pixels. The whole WFS and associated optics were placed on a mechanical slide, allowing translation in one axis across the 2′ field covered by the

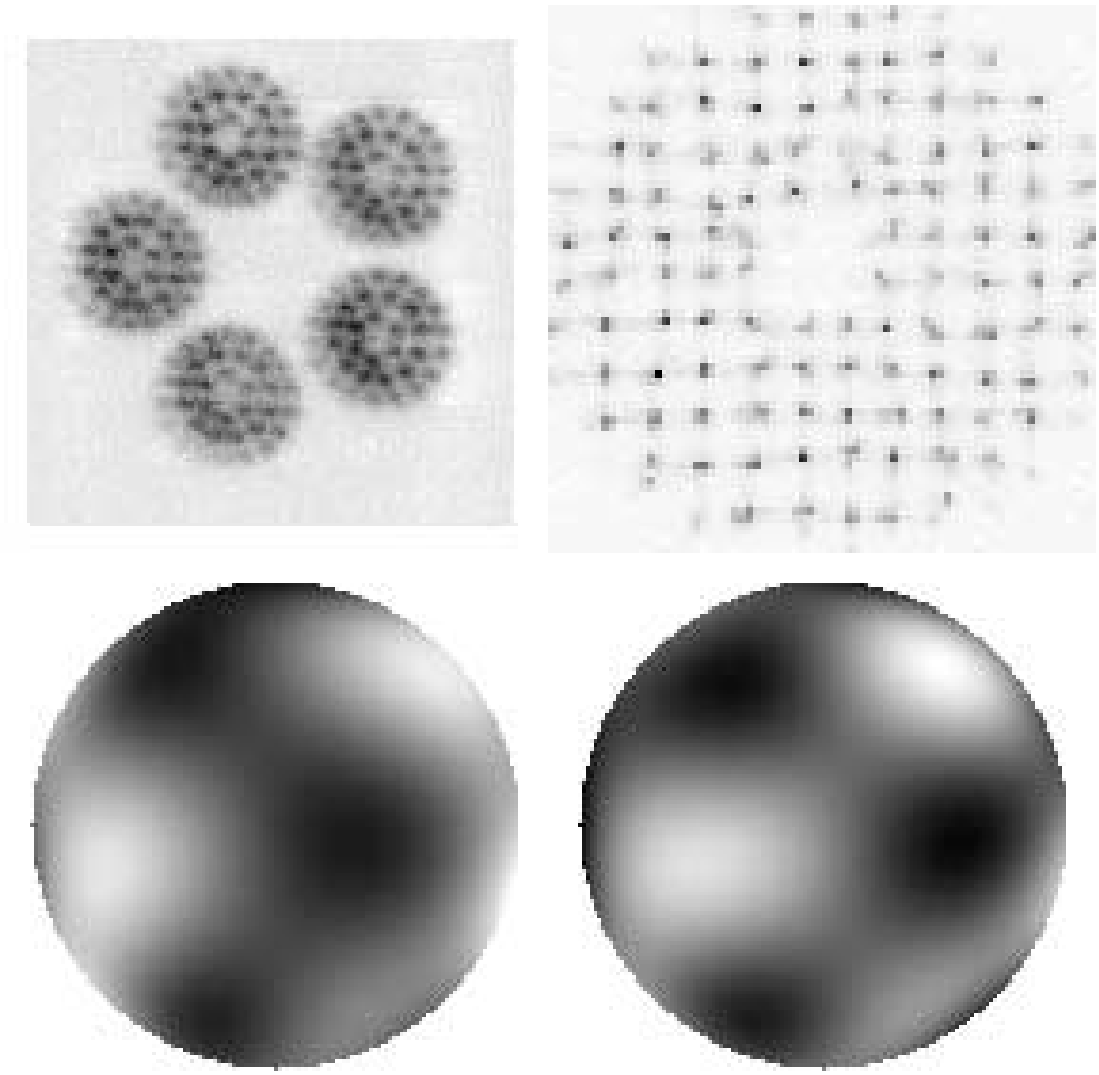

FIG. 1.—Examples of the WFS data. The top panels show the WFS outputs, with the RLGS sensor on the left and the star WFS on the right. The bottom panels show the corresponding wavefronts reconstructed to the sixth Zernike order. The RLGS reconstruction is the average of the five individual wavefronts. [*This figure is available as an mpeg file in the electronic edition of the Journal.*]

beacons. In practice, the telescope is offset a prescribed angle from the nominal stellar coordinates, and the WFS is moved by a corresponding angle in order to reacquire the star.

In operation, both sensors are run simultaneously but asynchronously, with the latter sensor providing measurements of the true stellar wavefront aberration to which reconstructions derived from the recorded RLGS signals can be compared. The star WFS was typically run at its maximum unbinned frame rate of 108 frames s^{-1}, with the RLGS sensor running at approximately half that frame rate. Data capture was externally registered in time by the use of synchronized flashing LEDs placed in front and to the side of each camera running at approximately 1 Hz.

3. OBSERVATIONS AND ANALYSIS

3.1. *Photometric and Imaging Performance of the RLGS Wavefront Sensor*

We have quantified the return flux from the RLGSs using observations of the spectrophotometric standard star HD 192281 made through a filter of 3 nm equivalent width centered on 532 nm. To do so, the prism array defining the subapertures in the RLGS WFS was replaced with a flat optic of the same construction, and the telescope was refocused to account for the substantial difference in stellar and beacon conjugates. The detected quantum efficiency of the WFS, including the telescope, optics and detector, was found to be 15%. Throughput of the beam projector optics was estimated at 73% from measurements of each element individually.

During observations of the RLGSs, the detected return flux at zenith was 1.1×10^5 photons m^{-2} J^{-1} over a range gate of 20–29 km. Accounting for our estimated efficiencies in both the outgoing and incoming beams, this amounts to 1.0×10^6 photons m^{-2} at the telescope aperture per joule at the output of the beam projector. The expected flux has been calculated from the lidar equation (Hardy 1998, p. 222) and the atmospheric transmission (Allen 2000), taking into account the atmospheric temperature and pressure profile measured by a routine meteorological balloon flight from nearby Tucson International Airport at approximately the same time as the observations. The agreement, within 2%, is good—fortuitously so, since the uncertainty in our estimate of the projected power is 10%–20%, dominated by uncertainty in the calibration of the lasers' built-in power meters. The return flux is as bright as a star of $m_v = 9.9$ seen

through a V filter and is similar to the range of returns from sodium beacons: Ge et al. (1998), for instance, measured 1.2×10^6 photons m^{-2} J^{-1}.

An unusual problem with the CCD in the RLGS WFS prevented the formation of sharp images. The typical FWHM of the Shack-Hartmann spots was found to be 4.4 pixels (equivalent to 3.″7) when images of the beacons recorded independently on a separate acquisition camera were measured to have a FWHM of ~1.″5. A replacement chip has since been installed that shows no sign of this blurring. The spot separation, set by the WFS optics, was just 4″, so that there was substantial overlap of neighboring spot images. An iterative deconvolution algorithm was required to recover usable spot positions. Furthermore, the increase in width reduced the signal-to-noise ratio (S/N) of the determination of each spot's position by a factor of ~2.5. An examination of the power spectral densities of the reconstructed modal amplitudes from the RLGSs showed that frequencies above 15 Hz were dominated by noise rather than by atmospheric signal. In the following analysis, therefore, a low-pass filter with a sharp cut at 15 Hz was applied to the data.

3.2. *Comparison of Laser and Natural Star Wavefronts*

Wavefront data were recorded during a 2 hr period on 2004 September 30, during which the seeing, 1.″0 in the V band, was worse than the median for the telescope. The recorded data are frames from the RLGS and star WFS cameras in near-continuous sequences of 9 s. Figure 1 shows sample frames taken simultaneously from the two cameras and the corresponding reconstructed wavefronts, which in the case of the RLGSs is the average of the five individual reconstructions. Both reconstructions are complete for the 25 modes in Zernike radial orders 2–6, although the resolution of the star WFS would allow more modal amplitudes to be calculated. Overall tip and tilt are, of course, not recovered from the lasers because of unknown beam motion in the upward paths.

Reconstructions of three individual modes as they evolve in time over a period of 3 s are shown, by way of example, in Figure 2. Values for the modal amplitudes for the average of the five beacons and the simultaneous values from a star near the center of the RLGS field are plotted. The generally good agreement indicates the presence of a strong ground layer. Aberration very close to the telescope's aperture would be common to all five RLGSs and the star and so would contribute in the same way to the variation of the modes. On the other hand, high-altitude turbulence would be sampled differently by the six light beams and would lead to the differences in the recovered amplitudes.

By subtracting the average RLGS wavefront from the stellar wavefront, one can obtain a quantitative estimate of the degree of correction possible with a simple ground-layer correcting scheme in which a DM conjugate to the telescope pupil is driven in response to the averaged beacon signals. Figure 3 shows the result for a 3 s sample of data. In general, we find that both the mean and the variance of the aberration are substantially reduced. We have investigated the potential for such correction for stars at several locations across the RLGS field. The geometry of the beacons and the positions of the stars in the field used for this study are laid out in Figure 4.

For the five positions of the star, Table 1 shows the measured stellar wavefront aberration averaged over all the Zernike modes in each order, both before and after subtraction of the average RLGS wavefront. The value of r_0, deduced from the image motion of the Shack-Hartmann spots in the stellar WFS and scaled to 500 nm wavelength, is also shown. The overall degree of correction varies from 40% near the center to 33% just outside the field covered by the RLGSs.

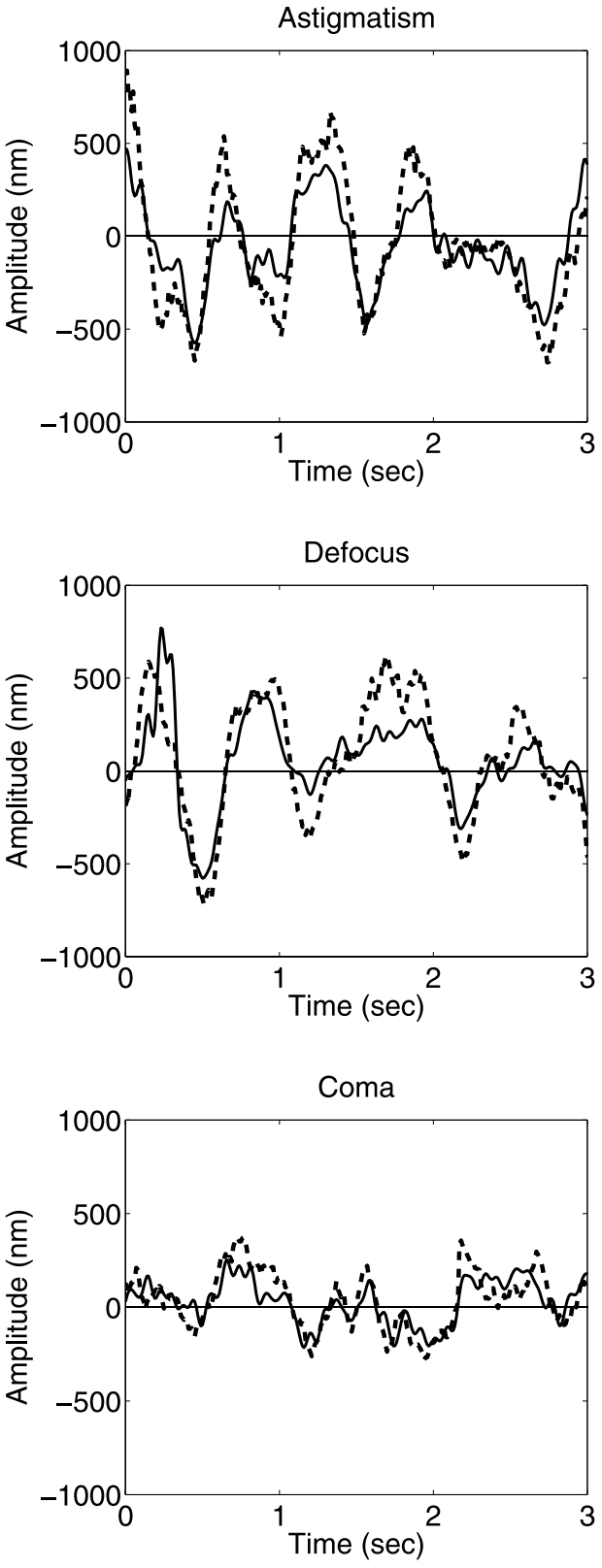

FIG. 2.—Examples of the reconstruction of three Zernike modal amplitudes from the natural star (*dashed line*) and the average RLGS signal (*solid line*).

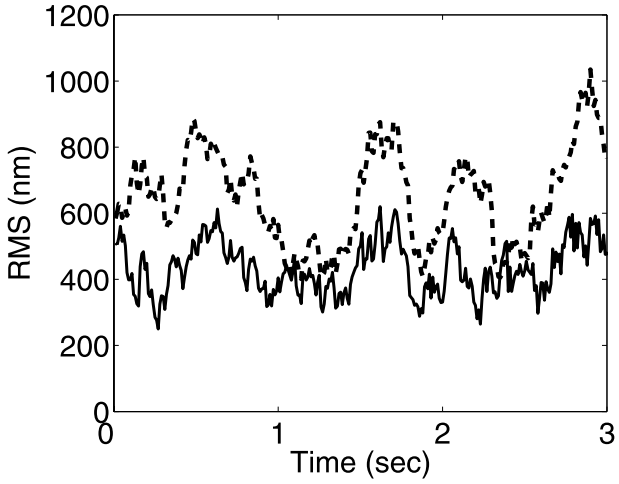

FIG. 3.—Wavefront aberration averaged over the 6.5 m pupil for a representative sample of data. The dashed line shows the total for the reconstructed modes in Zernike orders 2–6 in the stellar wavefront. The solid line shows the residual after subtraction of the average RLGS wavefront.

TABLE 1
WAVEFRONT ABERRATION BEFORE AND AFTER CORRECTION

Zernike Order	Set 1 (nm)	Set 2 (nm)	Set 3 (nm)	Set 4 (nm)	Set 5 (nm)
2.....	462	572	513	571	559
	255*	316*	308*	349*	343*
3.....	308	404	365	383	379
	198*	238*	226*	246*	258*
4.....	223	285	261	276	269
	142*	181*	168*	184*	190*
5.....	183	220	207	220	220
	140*	166*	152*	168*	168*
6.....	159	184	175	194	170
	116*	143*	130*	154*	143*
2–6.....	645	809	732	797	778
	397*	487*	463*	518*	518*
r_0 (cm).....	12.1	9.0	10.3	9.2	9.8

NOTES.—The rms stellar wavefront aberration averaged over the modes of each Zernike order; asterisks denote values after correction by the average RLGS signal. The sum over all measured orders is shown near the bottom, and the last row reports the observed value of r_0 at 500 nm wavelength.

Because the seeing varied significantly over the 2 hr period spanned by these observations, a direct comparison of wavefront correlation versus field angle is possible only by scaling the results to a common value. Figure 5 shows the results graphically, where the rms wavefront values in Table 1 have been scaled by a factor $(r_0/10.1\ \mathrm{cm})^{5/6}$, to the average value of r_0 of 10.1 cm seen during the observations. The greatest improvement is seen in the lowest orders, which is to be expected both because the amplitudes of the lower order modes have larger variance and are therefore sensed with greater S/N and because their angular correlation scale is larger, and therefore correction extends to a higher altitude than for modes with high spatial frequency. We also note that random noise in the reconstructions would preferentially appear as differences among the five RLGS signals, and so our estimate of the correlation between the natural star and mean LGS wavefronts is conservative.

3.3. *Vertical Distribution of Turbulence*

In a simplified model in which the vertical distribution of turbulence is characterized by just two regimes, one near the ground that is well corrected and the other at high altitude that is not corrected, one can readily calculate from our data the division of power in the aberration between the two. Under the assumption of a Kolmogorov spectrum with an infinite outer scale, the mean square wavefront error in orders 2–6 is $0.118(D/r_0)^{5/3}$ rad^2 (Hardy 1998, p. 96). A deficit of power is observed in the two tilt modes seen by the natural guide star (NGS) WFS, which we attribute to a finite outer scale, but in second and higher orders, the effect is small. In these orders, the overall average ground-layer corrected residual error inside 70″ radius is 464 nm, after the scaling to the mean seeing condition, yielding a value of r_0^{FA} for the uncorrected free atmosphere of 21.7 cm. The ground layer, then,

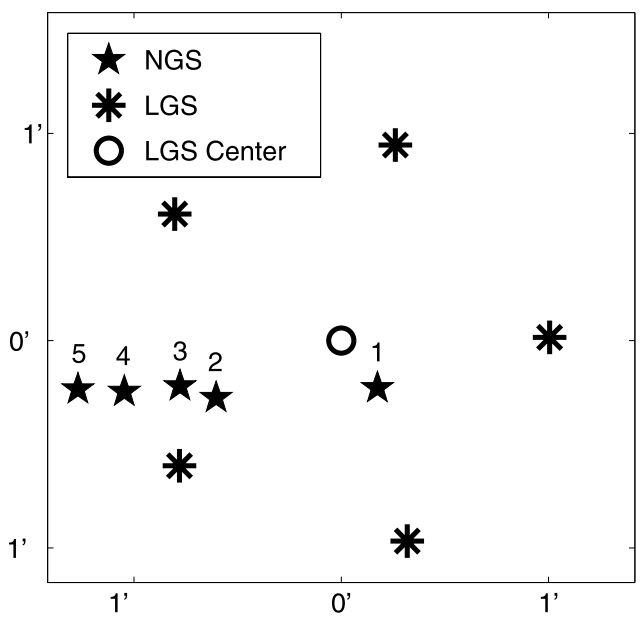

FIG. 4.—Geometry on the sky of the RLGSs used to measure the effect of boundary-layer wavefront sensing. The labeled positions of the natural star for which data were recorded are separated from the geometric center of the RLGS constellation by 17.″2, 39.″8, 48.″5, 64.″5, and 77.″5, respectively.

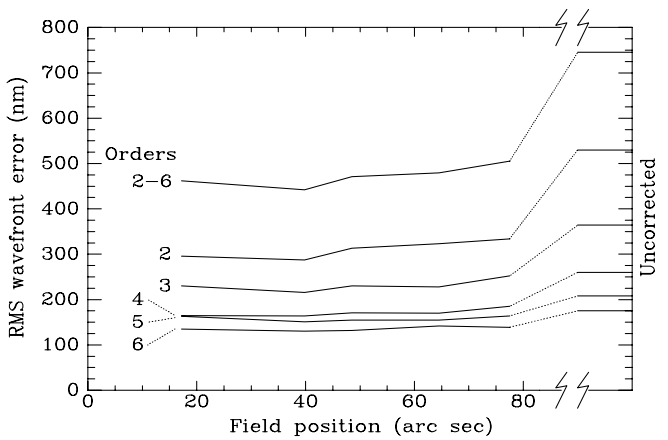

FIG. 5.—Graph of the rms residual error in the stellar wavefront after subtraction of the average beacon wavefront measurement. The plotted lines show the residual in all the modes of Zernike radial orders 2–6, averaged over time, and the contributions of each order separately. The short lines on the right represent the uncorrected rms wavefront aberrations. The points at each field angle represent averages of 9 s of data, and in each case the data have been scaled to the mean r_0 seen during the observations of 10.1 cm at 500 nm wavelength.

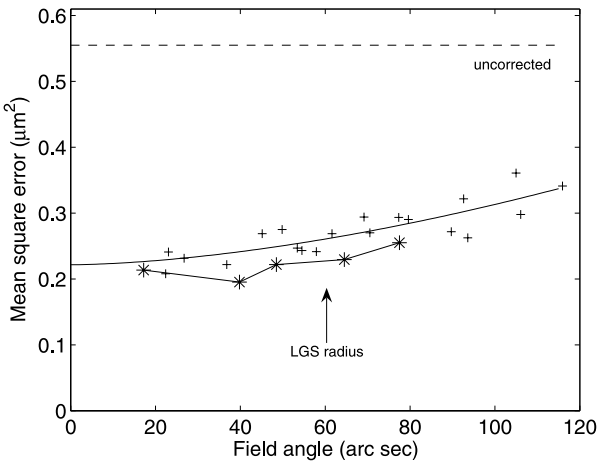

FIG. 6.—Mean square residual wavefront aberration (*plus signs*) after correction of the stellar wavefronts by simultaneous wavefronts from each of the RLGSs, taken singly, as a function of the angular separation of the star and beacon. A fit to a 5/3 power law is shown as the solid curve. The asterisks reproduce the top line of Fig. 5, showing the correction obtained from the average of the beacon wavefronts from the same data. The dashed line shows the mean square aberration in the uncorrected stellar wavefronts.

is characterized by $r_0^{\rm GL} = 12.3$ cm. This division of power of approximately two-thirds in the boundary layer and one-third in the free atmosphere is consistent with typical conditions at other sites (Verin et al. 2000).

The thickness of the boundary layer is an important parameter that sets the corrected angular field of GLAO and about which very little is known from current site surveys. Only recently have techniques been developed, such as SODAR (sound detection and range; Skidmore et al. 2004) and SLODAR (slope detection and range; Wilson 2002), that address the detailed structure of the lowest levels of turbulence.

The turbulence-weighted mean height of the ground layer, $h^{\rm GL}$, on the night of the observations can be estimated from the anisoplanatic behavior of the star and RLGS wavefronts. Figure 6 shows the mean square difference, as a function of angular separation, between the stellar wavefront and the simultaneous wavefront seen by four of the RLGSs separately. One beacon, which gave wavefronts noticeably noisier than the other four, has been omitted. All 20 pairings of the five star positions and RLGSs are plotted, after the same scaling to uniform r_0 as above. Also shown is a fitted curve of the form $y = a + b\theta^{5/3}$, the expected behavior of the anisoplanatic error. The fitted value of b is 42.5 ± 3.4 nm^2 arcsec$^{-5/3}$, where the uncertainty bounds an increase of 1 σ in the χ^2 fit metric. This corresponds to an isoplanatic angle for the sensed boundary layer only of $\theta_0^{\rm GL} = 20 \pm 1''$ at 500 nm wavelength. The isoplanatic angle is related to $h^{\rm GL}$ through the standard formula $\theta_0 = 0.314 \cos\zeta (r_0/h)$ (Hardy 1998, p. 103), where ζ is the zenith angle. Taking the mean value for these observations of $\cos\zeta = 0.95$, we find $h^{\rm GL} = 380 \pm 15$ m for the boundary-layer turbulence.

3.4. *Projected GLAO Gain with Single and Multiple RLGSs*

Under conditions of turbulence dominated by the ground layer, represented by our data, useful correction of seeing over a field of several arcminutes would be obtained with a simple correction system using just one Rayleigh beacon. By extrapolation of the curve of Figure 6, we find that the rms aberration would be improved out to an angle, set by $\theta_0^{\rm GL}$, of $\sim 2'.5$ where the mean square residual caused by angular decorrelation of the ground layer equaled the contribution from the uncorrected free atmosphere. For such a simple correction system, the Rayleigh laser would be preferred over a sodium laser, because it weights the ground layer more strongly than it does the decorrelated higher layers. This is the approach adopted by the Southern Astrophysical Research (SOAR) Telescope (Tokovinin et al. 2003).

Wavefront correction with multiple beacons would perform better over wide fields. Averaging the beacon signals leads to a higher rejection of free atmosphere aberration. Correction of stellar wavefronts in the direction of any given beacon would therefore be worse than if the signal from the beacon were used on its own. Over the field enclosed by the beacons, however, the wavefront compensation is expected to be more uniform. This effect, small but appreciable for the narrow constellation diameter we used, can be seen in the bottom trace in Figure 6, where we superpose the residual error after correction with orders 2–6 from the multibeacon average from Figure 5. The improvement at $1'$ radius is 13%.

4. MULTIBEACON SYSTEMS FOR CURRENT AND FUTURE LARGE TELESCOPES

4.1. *Practicality of Multibeacon Systems*

Implementation of practical AO systems with even one laser beacon has proven difficult. Sodium resonance systems were first proposed by Happer & MacDonald (1983) yet are only now starting to be scientifically productive. As a result, the concepts required for ELTs, which must rely on still more complex systems with multiple beacons to realize their unique high-resolution potential, have been even slower to develop.

Our first steps with a multibeacon system give encouragement that the engineering difficulties can be overcome. The laser WFS system was designed to be as simple as possible, yet in its early stages it has already proven capable of tracking the evolution of turbulence through sixth-order Zernike modes over a 6.5 m aperture. After the development of full tomographic reconstruction, correction to this degree in a closed-loop implementation of LTAO would yield the diffraction limit at the L band and longward, where the MMT is particularly powerful because of the low thermal background afforded by its adaptive secondary mirror.

A closed-loop system with broad scientific application would require response faster than the 15 Hz limit of the present data and smaller subapertures to provide correction at shorter wavelengths. We plan to increase the resolution of our RLGS WFS to 60 subapertures, for correction reaching down to the H band. Replacement of the CCD in that sensor to overcome the electronic blurring is expected to allow a substantial, although as yet unquantified, improvement. Photon noise does not set a practical limit; our measured flux at the WFS of 1.1×10^5 photons m^{-2} J^{-1} scales to 470 photons per subaperture per frame at the higher resolution and a rate of 500 frames s^{-1}, adequate for full correction in the K band. We also envision a further factor of 2.5 increase in photon flux by use of one 15 W laser for each beacon, which would allow operation through the H band. We note that the required beacon fluxes do not scale with aperture. Since the sodium beacons needed for ELTs yield about the same photon flux per watt, they need be no more powerful.

4.2. *Multiple Beacon Concept for the Giant Magellan Telescope*

The primary motivation for our work has been to understand the implementation of multibeacon AO for the 25 m GMT (Johns et al. 2004). Like the MMT, the GMT will be equipped with an adaptive secondary mirror for large-field GLAO correction and

optimum performance in the thermal infrared. Of particular value has been the realization that LTAO and GLAO can be considered as the extremes of a continuum provided by beacon constellations of variable diameter. The minimum diameter is that necessary for the beams to probe the cylindrical volume traversed by light from a star on-axis, 1.′5 for both the MMT with Rayleigh beacons and the GMT with sodium beacons. The maximum is $\sim 10'$ for wide-field GLAO. In the multibeacon implementation at the GMT, a single set of six beacons and six WFSs will be configured to cover this range of angles in both the projection and sensing systems.

The GMT's AO system will incorporate features proven valuable in the MMT prototype. For example, the constellation of beacons will rotate about the telescope axis in order to counter field rotation. This is done at the MMT by turning the hologram that splits the single laser beam into five. At the GMT, where we anticipate a separate laser for each sodium LGS, the same task will instead be done with a K mirror. The sensing system will be fed by reflection from an 8′ diameter dichroic mirror located above the direct Gregorian focus and will incorporate a set of six articulated periscopes to feed light from the variable-diameter constellation to fixed sensors. Such periscope optics are used now in the MMT, with a fixed reduction from 2′ to 1′.

Perspective elongation of the WFS spots will be significant, $\sim 4.''5$ in the outer subapertures of the GMT. Among several solutions proposed (Beckers 1992; Beckers et al. 2003; Ribak & Ragazzoni 2004; Baranec et al. 2005), our same dynamic refocus method at 5 kHz proven at the MMT could also be used with pulsed sodium lasers. The mechanical requirements for dynamic refocus on the larger telescope are not substantially more challenging than those already met at the MMT (Milton et al. 2003).

4.3. *RLGS Constellations for* 8 m *Class Telescopes*

The question arises whether a Rayleigh beacon constellation could be used as an alternative to a single or multiple sodium beacon for all AO operations at an 8 m telescope. While a single sodium beacon yields a good solution for the wavefront in the direction of the beam, the corrected field is small, limited by the usual angular anisoplanatism, and neither GLAO nor MCAO is possible. Multiple sodium beacons, the route being taken by the Gemini Observatory (Ellerbroek et al. 2003), would add these capabilities, but at a high cost: the lasers are at present more than an order of magnitude more expensive than YAG lasers of the same power.

Implementations of tomography with RLGSs have been studied in simulation. Lloyd-Hart et al. (2002) modeled LTAO on an 8.4 m telescope with beacons range-gated from 16 to 30 km. The corrected field of view remains small, but the axial *K*-band Strehl ratio was 0.55, comparable to performance predictions for 8 m telescopes with a single sodium beacon (Viard et al. 2000) and the values now achieved in practice with a sodium beacon on the 3 m Shane telescope (Gavel et al. 2003). Although we have yet to simulate the comparison directly, we believe that it could be possible for LTAO with Rayleigh beacons to improve on the performance of a single sodium beacon. This is because the beacons could be arranged to provide 100% sampling of the atmosphere up to a height above almost all of the turbulence. This contrasts with the single sodium beacon case, in which pupil coverage begins to drop immediately above the telescope and falls off with height. A fraction of the turbulence is therefore unsensed, and more importantly, an unknown radial shear is introduced into the measured wavefront.

Figure 7 illustrates the fractional coverage of the area filled by on-axis starlight as a function of height by a single sodium beacon at 95 km range and a regular pentagon of Rayleigh beacons

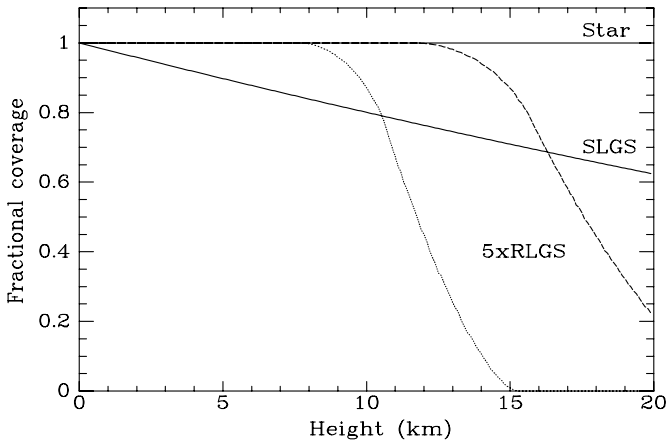

FIG. 7.—Fractional intersection vs. height of the area covered by light from an axial star and three LGS beacon arrangements: a single axial sodium laser guide star (SLGS) at 95 km range and pentagonal constellations of Rayleigh laser guide stars (RLGSs). We show the cases of a 6.5 m aperture with the RLGSs on a 60″ radius at 24 km range (*dotted line*) and an 8.0 m aperture with RLGSs on a 43″ radius at 30 km range (*dashed line*).

in two cases. For the present constellation diameter of 2′ and mean height of 24 km above a 6.5 m aperture, complete coverage is available to 8 km. SCIDAR (scintillation detection and range) measurements above nearby Mt. Graham at the site of the Large Binocular Telescope (McKenna et al. 2003) indicate that this is typically above 75% of the integrated C_n^2. Also shown is the case of a telescope of 8.0 m diameter, where the beacon diameter has been set to 86″, which gives the greatest height for full coverage, and the beacons projected to a mean range of 30 km. There full coverage extends to 12 km. Even above that height, the Rayleigh beacons continue to provide better atmospheric sampling than a single sodium beacon up to 16.3 km, high enough to capture essentially 100% of the integrated C_n^2. Furthermore, tomographic reconstruction from the multiple Rayleigh beacons could in principle remove much of the focal anisoplanatism error inherent in the single sodium beacon measurement.

Lloyd-Hart & Milton (2003a) have simulated the performance of MCAO on the MMT using two DMs and five Rayleigh beacons. They find that correction to the diffraction limit in the near-infrared is achieved over a 1′ field, if the RLGSs are each sampled at two distinct heights. Modeling by De la Rue & Ellerbroek (2002), comparing MCAO systems on an 8 m telescope relying on Rayleigh beacons, sodium beacons, and a combination of the two, came to the same conclusion. That study further shows that the performance of the doubly sampled Rayleigh system approaches that of sodium beacons in the same geometry. In practice, such a system of Rayleigh beacons could be built with polarized lasers and a Pockels cell to switch each returning beam from one WFS to another as each laser pulse rose through the atmosphere. The lasers, optics, and detectors to implement the scheme would be still much cheaper than the lasers needed to construct an equivalent with sodium lasers.

Rayleigh beacons at 30 km of similar brightness to those at 24 km at the MMT could be made with individual lasers of 15 W. The results of the models described above suggest that a system on an 8 m telescope that deployed five 15 W lasers, each dedicated to a single beacon, would allow the full range of LTAO, MCAO, and GLAO techniques to be implemented.

5. CONCLUSIONS

Our results show that a constellation of RLGSs would be a powerful tool for ground-layer adaptive correction when used to

drive the MMT's adaptive secondary mirror. Other large telescopes equipped with adaptive secondary mirrors and with similar boundary layers of ~500 m mean thickness could also benefit with much-improved *K*-band images expected from GLAO over a field as large as 10′ diameter.

The main consideration that remains unexplored so far by our experiments is the power of tomographic methods applied to multiple Rayleigh beacons to recover higher layer aberrations as well as the ground layer. Open-loop field tests to show the practicality of tomography are planned with the MMT system. Wavefronts will be reconstructed as Zernike modes on two metapupils at the ground and at high altitude. The choice of the upper altitude is not critical (Lloyd-Hart & Milton 2003b). The performance of LTAO will be evaluated by comparing direct measurements of natural star wavefronts in the center of the RLGS constellation with the integral of the tomographic solution along the same line of sight. In addition, the two-layer reconstructions will allow an early investigation of the performance of MCAO by exploring the agreement of the stellar and the integrated reconstructed wavefronts over the field enclosed by the RLGSs.

Our plans also call for closed-loop demonstrations of both GLAO and LTAO with the MMT's adaptive secondary mirror and the addition of a new real-time reconstructor computer recently received from Microgate S.r.l. Later, the addition of a second DM conjugated to high altitude will allow us to explore MCAO.

This work has been supported by the National Science Foundation under grant AST 01-38347 and the Air Force Office of Scientific Research under grant F49620-01-1-0383. We are grateful for the continued support of the MMT Observatory staff, particularly A. Milone, J. McAfee, and M. Alegria.

REFERENCES

Allen, C. W. 2000, in Allen's Astrophysical Quantities, ed. A. N. Cox (4th ed.; New York: Springer), 264
Angel, J. R. P., & Lloyd-Hart, M. 2000, Proc. SPIE, 4007, 270
Baranec, C., Bauman, B., & Lloyd-Hart, M. 2005, Opt. Lett., 30, 693
Beckers, J. M. 1988, in Very Large Telescopes and Their Instrumentation, ed. M.-H. Ulrich (Garching: ESO), 693
———. 1992, Appl. Opt., 31, 6592
Beckers, J. M., Owner-Petersen, M., & Andersen, T. 2003, Proc. SPIE, 5169, 123
Berkefeld, T., Soltau, D., & von der Lühe, O. F. H. 2004, Proc. SPIE, 5490, 260
Brusa, G., Miller, D. L., Kenworthy, M. A., Fisher, D. L., & Riccardi, A. 2004, Proc. SPIE, 5490, 23
Dekany, R. G., Britton, M. C., Gavel, D. T., Ellerbroek, B. L., Herriot, G., Max, C. E., & Véran, J.-P. 2004, Proc. SPIE, 5490, 879
De la Rue, I. A., & Ellerbroek, B. L. 2002, Proc. SPIE, 4494, 290
Ellerbroek, B. L., et al. 2003, Proc. SPIE, 4839, 55
Fugate, R. Q. 2003, Proc. SPIE, 4837, 934
Fugate, R. Q., et al. 1991, Nature, 353, 144
Gavel, D. T., Olivier, S. S., Bauman, B. J., Max, C. E., & Macintosh, B. A. 2000, Proc. SPIE, 4007, 63
Gavel, D. T., et al. 2003, Proc. SPIE, 4839, 354
Ge, J., Jacobsen, B. P., Angel, J. R. P., McGuire, P. C., Roberts, T., McLeod, B., & Lloyd-Hart, M. 1998, Proc. SPIE, 3353, 242
Georges, J. A., Mallik, P., Stalcup, T., Angel, J. R. P., & Sarlot, R. 2003, Proc. SPIE, 4839, 473
Hammer, F., et al. 2002, in Scientific Drivers for ESO Future VLT/VLTI Instrumentation, ed. J. Bergeron & G. Monnet (Garching: ESO), 139
Happer, W., & MacDonald, G. J. 1983, JASON Report JSR-82-106 (MacLean: MITRE Corp.)
Hardy, J. W. 1998, Adaptive Optics for Astronomical Telescopes (New York: Oxford Univ. Press)
Johns, M., Angel, J. R. P., Shectman, S., Bernstein, R., Fabricant, D. G., McCarthy, P., & Phillips, M. 2004, Proc. SPIE, 5489, 441
Langlois, M., Rimmele, T., & Moretto, G. 2004, Proc. SPIE, 5171, 187
Lloyd-Hart, M., Georges, J., Angel, R., Brusa, G., & Young, P. 2002, Proc. SPIE, 4494, 259
Lloyd-Hart, M., & Milton, N. M. 2003a, Proc. SPIE, 4839, 578
———. 2003b, J. Opt. Soc. Am. A, 20, 1949
McKenna, D. L., Avila, R., Hill, J. M., Hippler, S., Salinari, P., Stanton, P. C., & Weiss, R. 2003, Proc. SPIE, 4839, 825
Milton, N. M., Lloyd-Hart, M., Cheng, A., Georges, J., & Angel, J. R. P. 2003, Proc. SPIE, 5169, 238
Putnam, N., Snyder, M., Stalcup, T., & Angel, R. 2004, Proc. SPIE, 5490, 1138
Ragazzoni, R., Marchetti, E., & Rigaut, F. 1999, A&A, 342, L53
Ragazzoni, R., Marchetti, E., & Valente, G. 2000, Nature, 403, 54
Ribak, E. N., & Ragazzoni, R. 2004, Opt. Lett., 29, 1351
Rigaut, F. 2002, in ESO Conf. Proc. 58, Beyond Conventional Adaptive Optics, ed. E. Vernet et al. (Garching: ESO), 11
Skidmore, W., et al. 2004, Proc. SPIE, 5489, 154
Stalcup, T. E., Georges, J. A., Snyder, M., Baranec, C., Putnam, N., Milton, N. M., Angel, R., & Lloyd-Hart, M. 2004, Proc. SPIE, 5490, 1021
Tokovinin, A. 2004a, Proc. SPIE, 5382, 490
———. 2004b, PASP, 116, 941
Tokovinin, A., Gregory, B., Schwarz, H. E., Terebizh, V., & Thomas, S. 2003, Proc. SPIE, 4839, 673
Tokovinin, A., Le Louarn, M., & Sarazin, M. 2000, J. Opt. Soc. Am. A, 17, 1819
Tokovinin, A., Le Louarn, M., Viard, E., Hubin, N., & Conan, R. 2001, A&A, 378, 710
Verin, J., et al. 2000, Gemini Obs. Internal Rep. RPT-AO-G0094 (Tucson: Gemini Obs.)
Viard, E., Hubin, N., & Le Louarn, M. 2000, Proc. SPIE, 4007, 106
Wilson, R. W. 2002, MNRAS, 337, 103
Wizinowich, P. L., et al. 2004, Proc. SPIE, 5490, 1